Near-field vector intensity measurements of a small solid rocket motor

Kent L. Gee[a] **and Jarom H. Giraud**
Department of Physics and Astronomy, Brigham Young University, Provo, Utah 84602
kentgee@byu.edu, jaromgiraud@gmail.com

Jonathan D. Blotter
Department of Mechanical Engineering, Brigham Young University, Provo, Utah 84602
jblotter@byu.edu

Scott D. Sommerfeldt
Department of Physics and Astronomy, Brigham Young University, Provo, Utah 84602
scott_sommerfeldt@byu.edu

Abstract: Near-field vector intensity measurements have been made of a 12.7-cm diameter nozzle solid rocket motor. The measurements utilized a test rig comprised of four probes each with four low-sensitivity 6.35-mm pressure microphones in a tetrahedral arrangement. Measurements were made with the rig at nine positions (36 probe locations) within six nozzle diameters of the plume shear layer. Overall levels at these locations range from 135 to 157 dB re 20 μPa. Vector intensity maps reveal that, as frequency increases, the dominant source region contracts and moves upstream with peak directivity at greater angles from the plume axis.

PACS numbers: 43.50.Nm, 43.58.Fm [MS]
Date Received: February 18, 2010 **Date Accepted:** May 3, 2010

1. Introduction

The characterization of high-speed, high-temperature jet aeroacoustic noise sources requires that the source locations and amplitudes be inferred from measurements outside the flow. Examples of phased-array methods implemented for determining these sources include polar correlation techniques,[1,2] beamforming methods,[3,4] and, recently, near-field acoustical holography.[5] The purpose of this Letter is not to fully compare or debate the relative merits of these methods, but rather to present results from a different approach that uses near-field vector intensity measurements to characterize jet aeroacoustic sources.

The use of multidimensional intensity probes has not yet seen broad application to jet aeroacoustics. Ventakesh *et al.*[4] mention the use of a one-dimensional intensity probe to validate the application of a statistical beamforming method to a subsonic jet. In addition, Yu *et al.*[6] have recently described a surface-normal intensity inverse method to characterize source regions with application to aeroacoustics.

The most extensive use of vector acoustic intensity to study jet noise characteristics has been by Jaeger and Allen,[7] who applied a two-dimensional intensity probe to the characterization of unheated Mach 0.2–0.6 jets. They traversed their probe along different centerline offsets and used the intensity vector angles to locate the apparent aeroacoustic source regions. Given their jet flow conditions, the intensity levels reported were relatively low and a compact source region was reported. Despite some issues regarding the calculation of intensity levels and interpretation of active intensity in the near field, Jaeger and Allen's initial work provides insight into the merits of intensity measurements in jet aeroacoustic source characterization.

[a]Author to whom correspondence should be addressed.

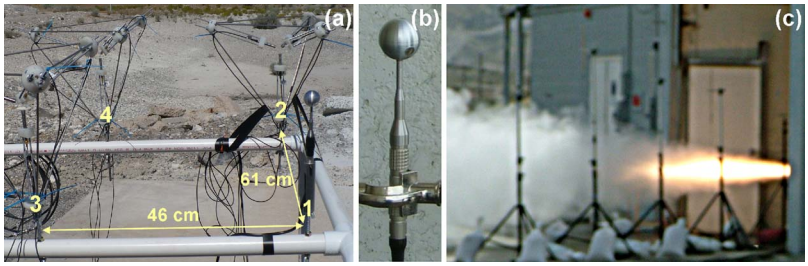

Fig. 1. (Color online) (a) Intensity test rig with the four tetrahedral probes labeled and distances indicated. (b) Close-up of GRAS-built spherical probe. (c) One of the motor firings with tripod-mounted mid-field microphones.

In this Letter, near-field vector intensity measurements of the noise generated by a small solid-fuel rocket motor are described. The measurements were part of an effort to develop an energy-based acoustic probe suitable for near-field noise measurements of statically-fired rockets.[8] Following a description of the tests conducted with some discussion of overall and spectral data, vector intensity results are presented and analyzed.

2. Test setup and level-based results

A PVC pipe test rig held four tetrahedral intensity probes [see Fig. 1(a)] of two different designs. Probe 1 was the custom GRAS-built probe prototype. The probe contains four phase-matched 6.35-mm GRAS 40BH microphones in a tetrahedral configuration flush mounted on a machined aluminum sphere with a diameter of 2.54 cm [see Fig. 1(b)]. The preamplifiers reside inside the sphere and the four data channels are carried through a single seven-pin LEMO cable before being broken out into four separate channels and powered by two GRAS 12AA power supplies. Probes 2, 3, and 4 consist of 6.35 mm

Type 1 microphones that were intensity-calibrated and held in a tetrahedral configuration with the same microphone separation distance as the spherical probe. Probe 2 used GRAS 40 BH microphones, whereas Probes 3 and 4 used low-sensitivity ($\sim$0.5 mV/Pa) GRAS 40 BD microphones. These probes and their performance in preliminary large rocket motor tests are discussed further in Ref. 8.

The tests were conducted at ATK Space Systems' small motor test facility in Promontory, Utah, where rocket motors filled with seven lbs of the solid propellant used in ATK's reusable solid rocket motor (RSRM) are tested for thrust equivalency [see Fig. 1(c)]. Each of these test motors burns for approximately 2.5 s through a 12.7 cm exit diameter conical nozzle. The motor is positioned on a test stand such that the motor axis is 81 cm off the concrete pad. Time waveform data from each channel were simultaneously acquired with 24-bit National Instruments PXI-4462 cards at a sampling rate of 204.8 kHz.

During the test, the probe centers were placed at a height of 96 cm and the rig moved to different distances along a 12° line parallel to and horizontally offset 15 cm from the shear layer at the centerline. Two motor firings were recorded at each rig location to verify data consistency. The probe locations and overall sound pressure level (OASPL) are depicted in Fig. 2. In Fig. 2(a), the OASPL is shown as an interpolated two-dimensional color map. In Fig. 2(b), the OASPL is plotted for all four probes and each motor burn as a function of scaled downstream distance (y/D). The OASPL values indicate a maximum source location of y/D no further downstream than 10–12 diameters. Note that the measured OASPL values are slightly less than they would be if the rig had been aligned along the centerline rather than with a 15 cm vertical offset, which was done to provide a vertical intensity component for probe performance verification. However, in the context of source localization, the effect of the offset is shown to be minimal in the next section.

Before moving to the intensity results, it is important to verify the equivalence of each motor firing, otherwise the method of measuring the plume environment asynchronously is inappropriate. Of course, the smooth variation in OASPL and the consistency between the two

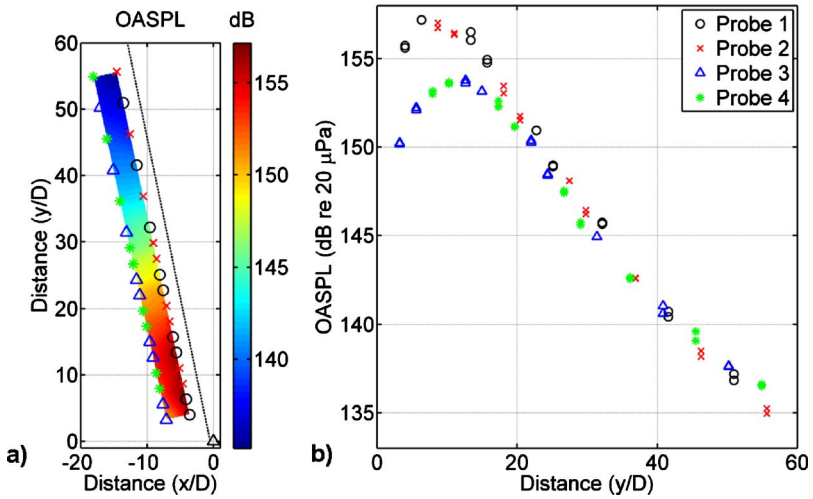

Fig. 2. (Color online) (a) Interpolated overall sound pressure level (OASPL) map showing the locations of the tetrahedral intensity probes, which are labeled in Fig. 2(b) and described further in the text. OASPL shown is the average of two different motor firings for location. (b) OASPL at the four probes at the nine test rig locations for both motor firings at each position. Note the very small variation between motor firings.

motor firings for each position in Fig. 2(b) (less than 0.2 dB for many positions) suggest that the each motor represents a comparable acoustic source. However, this is confirmed through the use of stationary, tripod-mounted GRAS 40 BD microphones as shown in Fig. 1. For example, Fig. 3 shows the power spectral density at a tripod-mounted mid-field microphone located at $(x,y,z)/D=(-21.6,43.2,24.6)$ for each of the 18 motor firings. The spectra overlay each other with extreme consistency even in the frequency regions of the ground-induced interference nulls occurring between 200 and 1000 Hz. In a confirmation of the overall level consistency from Fig. 2, the OASPL at this microphone has a standard deviation of 0.2 dB. Note that visually smoothing the interference nulls by extrapolating the positive and negative spectral slopes results in an approximate peak-frequency region of about 400–500 Hz at this location. This result is useful in the subsequent discussion of the vector intensity results.

3. Vector intensity results

The pressure data from the four tetrahedral probes have been used to calculate three-dimensional active intensity vectors at the nine rig positions. As is typically done with intensity

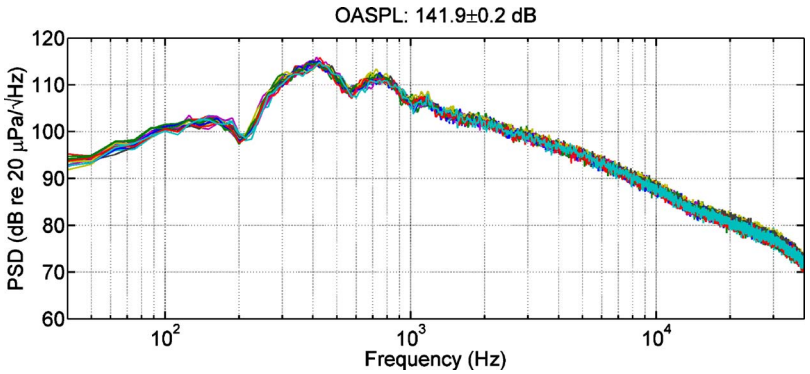

Fig. 3. (Color online) Power spectral density (PSD) at one of the mid-field microphones for all 18 motor firings, showing the consistency of the acoustic fields produced by the motors. The average and standard deviation of the OASPL is displayed at the top of the plot.

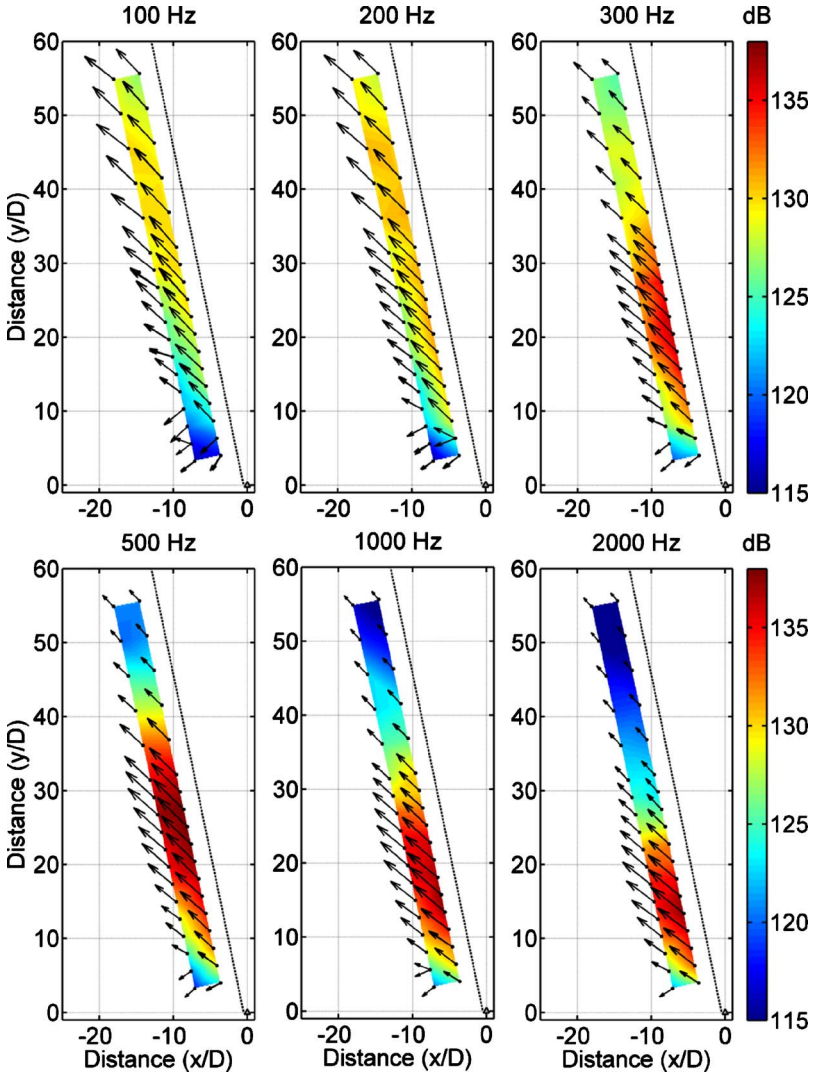

Fig. 4. (Color online) Representative total intensity level magnitude and *x*-*y* horizontal intensity vectors (lengths scaled by the fourth-root of the magnitude) for the small solid rocket motor firings. The vectors from each motor firing are shown. The approximate shear layer location is shown by the dashed line.

calculations, the finite-sum estimate for the pressure and the Euler equation-based finite-difference estimate of the particle velocity components are expressed in terms of cross spectra between various microphone pairs. The individual estimates are then weighted to provide the best least-squares estimate for each intensity component.[9]

Displayed in Fig. 4 are representative horizontal (*x*-*y*) intensity vectors from 100 Hz to 2 kHz, along with total intensity magnitude calculated from all three components. For convenient visualization, the vector magnitudes are normalized by the maximum intensity for that frequency and then compressed by displaying the fourth root of the intensity. Two-dimensional vectors are shown for simpler data visualization because the vertical intensity components were found to be generally small beyond the first rig position. As can be seen by comparing the horizontal vector lengths with the total magnitude level, neglecting the vertical intensity component despite not aligning the probe along the centerline does not appreciably influence con-

clusions about source locations in this case. Note that the vectors from both motor firings for each rig position are shown and essentially overlay each other except for a few locations in the vicinity of the nozzle. The maximum frequency has been conservatively limited to 2 kHz to minimize bias errors in the calculations due to finite-sum pressure averaging and scattering effects of the probes.

Several observations can be made from the results in Fig. 4. First, the vectors show that the apparent source region contracts and moves upstream as a function of frequency. This is consistent with past studies of jet noise and the results of far-field-based beamforming methods (e.g., see Ref. 3). Second, examination of the results shows evidence of refraction of the sound waves outside the plume. This is particularly evident for the 100 and 200 Hz results and possibly for all frequencies upstream of the dominant intensity locations (i.e., $y/D < 10$). (Another possible reason for the upstream behavior is discussed subsequently.) Near-field refraction is potentially important because far-field beamforming, correlation, and other related methods, which assume straight-ray propagation from source to receiver, could erroneously localize the apparent source location.

A third observation that can be made is a comparison between the apparent dominant source region for the maximum-intensity frequency and the OASPL. In Fig. 4, 500 Hz has the greatest intensity magnitude of the six frequencies shown. A rough extrapolation of intensity direction from the dominant source region to the mid-field microphone location whose PSD is shown in Fig. 3 explains the 400–500 Hz peak-frequency region of that microphone spectrum. However, the apparent source location for 500 Hz (>20 y/D) is significantly downstream than the maximum OASPL in Fig. 2. A comparison of Figs. 2 and 4 suggests an integrated effect of higher frequencies (e.g., >1 kHz) dominating the maximum OASPL-generating region despite being of lesser total intensity than 500 Hz.

An additional point to be made in examining the data regards the similar directions for all frequencies in the dominant intensity regions. For Probes 1 and 2 (closer to the plume), the vector angles, as measured relative to the downstream axis, range approximately between 44°–51°. They are systematically shallower for the lower frequencies than the higher frequencies. This range of angles and the increase of angle with frequency are consistent with the "standard chemical rocket" far-field peak directivity trends found in Ref. 10. In addition, these results are dramatically different from the Jaeger and Allen[7] study, which showed converging intensity vectors resulting in a relatively compact source region. This indicates a fundamentally different aeroacoustic source mechanism dominates the radiation for the case of this small rocket motor than their subsonic, unheated jet.

The intensity vector directions in Fig. 4 can also be examined in the context of the prevailing theory of jet noise. Tam and colleagues (e.g., see Ref. 11 references therein) have used far-field data and semi-empirical models to argue that there are two fundamentally different sources of noise within a jet plume: fine-scale turbulence and large turbulence structures. To summarize, the fine-scale turbulence radiates throughout the mixing layer as compact, uncorrelated sources with a broadly-shaped rounded noise spectrum, whereas the large structures radiate primarily downstream as a more coherent, extended source with a more peaked spectrum. Thus, the downstream radiation has characteristics associated with the large turbulence radiation whereas the sideline radiation is more dominated by fine-scale turbulence. The rapid transition in intensity vector direction near the nozzle could be near-field evidence of the two-source model. The downstream-pointing vectors are consistent with large-turbulence structure theory, whereas the sideline and upstream-pointing vectors could be evidence of fine-scale turbulence that radiates with less directionality. A larger measurement aperture extending farther upstream and outward from the source would be desirable to better study the near-field propagation and possibly corroborate Tam *et al.*'s far-field-based model.

4. Conclusion

This Letter has illustrated the capability of near-field intensity measurements to characterize source regions of rocket plumes and other high-thrust jet noise sources. The technique can be used to infer source locations from near-field measurements without the assumptions or more

extensive signal processing required by far-field phased array techniques. It can also be used to help establish transitions in time-averaged acoustical energy flow as a function of frequency from the near to the far fields. This would be instrumental in examining the applicability of the two-source jet noise model in the near, rather than the far, field.

Future work ought to include measurements and analysis of large-scale model-scale controlled jets with known source parameters in conjunction with other source localization methods. In addition, source locations have been inferred and discussed solely by visual inspection. Intensity-based inverse methods could be applied and/or further developed to more rigorously determine source characteristics.

Acknowledgments

This research was carried out in part under an STTR with STI Technologies and funded by NASA Stennis Space Center. Daniel Manwill fabricated the tetrahedral microphone holders and Alan Wall and Derek Thomas assisted with measurements. In addition, the support of ATK Space Systems Test Services, in particular, Dennis Beatty, Gary Roderick, Shyla Quinn, Chad Johnson, and Kevin Rees is gratefully acknowledged.

References and links

[1]H. V. Fuchs, "On the application of acoustic 'mirror,' 'telescope,' and 'polar correlation' techniques to jet noise source location," J. Sound Vib. **58**, 117–126 (1978).
[2]J. Panda, "Identification of noise sources in high speed jets via correlation measurements—A review," NASA Report No. CR-2005-213817, Glenn Research Center, Cleveland, OH, 2005.
[3]S. S. Lee and J. Bridges, "Phased-array measurements of single flow hot jets," NASA Report No. TM-2005-213826, Glenn Research Center, Cleveland, OH, 2005.
[4]S. R. Venkatesh, D. R. Poak, and S. Narayanan, "Beamforming algorithm for distributed source localization and its application to jet noise," AIAA J. **41**, 1238–1246 (2003).
[5]M. Lee and J. S. Bolton, "Source characterization of a subsonic jet by using near-field acoustical holography," J. Acoust. Soc. Am. **121**, 967–977 (2007).
[6]C. Yu, Z. Zhou, and M. Zhuang, "An acoustic intensity-based method for reconstruction of radiated fields," J. Acoust. Soc. Am. **123**, 1892–1901 (2008).
[7]S. M. Jaeger and C. S. Allen, "Two-dimensional sound intensity analysis of jet noise," AIAA Paper No. 93-4342.
[8]K. L. Gee, J. H. Giraud, J. D. Blotter, and S. D. Sommerfeldt, "Energy-based acoustical measurements of rocket noise," AIAA Paper No. 2009-3165.
[9]J.-C. Pascal and J.-F. Li, "A systematic method to obtain 3D finite-difference formulations for acoustic intensity and other energy quantities," J. Sound Vib. **310**, 1093–1111 (2008).
[10]K. M. Eldred, "Acoustic loads generated by the propulsion systems," NASA Report No. SP-8072, Langley Research Center, Hampton, VA, 1971.
[11]C. K. W. Tam, K. Viswanathan, K. K. Ahuja, and J. Panda, "The sources of jet noise: Experimental evidence," J. Fluid Mech. **615**, 253–292 (2008).